Temporal Mixture Analysis of Hypertemporal Antarctic Sea Ice Data in the Sense of Machine Learning

KOPRI Korea Polar Research Institute

AGU FALL MEETING San Francisco | 14–18 December 2015

C41D-0746

Junhwa Chi (jhchi@kopri.re.kr) and Hyun-Cheol Kim (kimhc@kopri.re.kr)
Department of Polar Remote Sensing, Korea Polar Research Institute, Incheon, Korea

Abstract

Hypertemporal image (HTI) is often used to exploit the seasonal characteristics of environmental phenomena such as sea ice concentration (SIC). However, it is difficult to analyse the long-term time series acquired at high temporal frequencies and over extensive areas. This study performed temporal mixture analysis (TMA), which is algebraically similar to spectral mixture analysis (SMA), but occurs in the time domain instead of the spectral domain. TMA was used to investigate the temporal characteristics of Antarctic sea ice. Because endmember (EM) selection is critical to the success of both SMA and TMA, it is important to select proper EMs from large quantities of HTI. In this study, a machine learning (ML) technique is incorporated in identifying EMs without prior information to address the limitations of previous research. A fully linear mixing model was then implemented in an attempt to produce more robust and physically meaningful abundance estimates. Experiments that quantitatively and qualitatively evaluated the proposed approaches were conducted. A TMA of high-temporal-dimensional data provides a unique summary of long-term Antarctic sea ice and noise-whitened reconstruction images via inverse processing. Furthermore, comparisons of regional sea ice fractions from experimental results enhance the understanding of the overall Antarctic sea ice changes.

1. Introduction

- Although Piwowar, Peddle, and Ledrew (1988) first investigated TMA by analysing long-term temporal remote sensing (RS) data that were generated using 9 years of monthly Arctic SIC data, simple statistics (e.g. mean, median, maximum and minimum) are used to derive pure temporal EM spectra from a sample set of image spectra. However this method may not properly capture the seasonal characteristics of sea ice because monthly data provide insufficient temporal information, and the temporal EMs generated by the purification process are not always collected on the same scale as the image data.
- In this study, ML techniques are used for TMA of Antarctic SIC to provide unique and summarized information of long-term time series in three steps.
  1) Use daily SIC data, which are similar to hyperspectral image data but are in different domain, to better seasonally characterize the Antarctic sea ice.
  2) Apply an ML-based endmember extraction (EE) algorithm to generate a collection of pure temporal signatures due to a lack of prior information on sea ice seasonality.
  3) Conduct quantitative/qualitative experiments, and discussed results to evaluate the proposed approaches.

2. Methodology

2.1 Datasets

- 36 years of daily SIC data from 1979 to 2014 provided by NSIDC (National Snow and Ice Data Center).
- 25-km spatial resolution in the polar stereographic projection.
- Linear interpolation was applied to SIC data from 1978 to 1987 to generate consistent daily time series throughout the time period.

2.2 Temporal mixture analysis (TMA)

- SMA assumes that the surface is dominated by a small number of such substances and can be modelled by representing the substance at sub-pixel levels.
- The main idea underlying TMA of HTIs is rooted in SMA. TMA assumes that the time series consist of several temporal components that represent the seasonal characteristics of the substances.
- Two general steps were employed to address the mixing problems:
  1) Identifying temporally unique signatures of pure components (temporal endmembers).
  2) Unmixing each pixel in the time series as a linear combination of EM fractional abundances.

2.3 Linear mixing models for TMA

- Assumptions:
  1) The temporal trajectories of seasonal sea ice are linearly independent.
  2) The pixels in the image line in linear spaces.
- Fully constrained linear unmixing (Heinz and Chang 2001):
  To find the fractional abundances (α) that minimize the pixel reconstruction error $\|\mathbf{x}-\mathbf{E}\alpha\|^2$, where $\mathbf{x}$ is a daily trajectory of HTI, $\mathbf{E}$ is a temporal EM matrix. The least squares solution is $\alpha=\left(\mathbf{E}^T\mathbf{E}\right)^{-1}\mathbf{E}^T\mathbf{x}$.
  Two constraints for each HTI pixel to estimate physically meaningful abundances:
  1) Non-negative: $\alpha_i \geq 0; \forall \alpha_i : 1 \leq i \leq q$ where q is the number of temporal EMs.
  2) Sum-to-one: $\sum \alpha_i = 1$

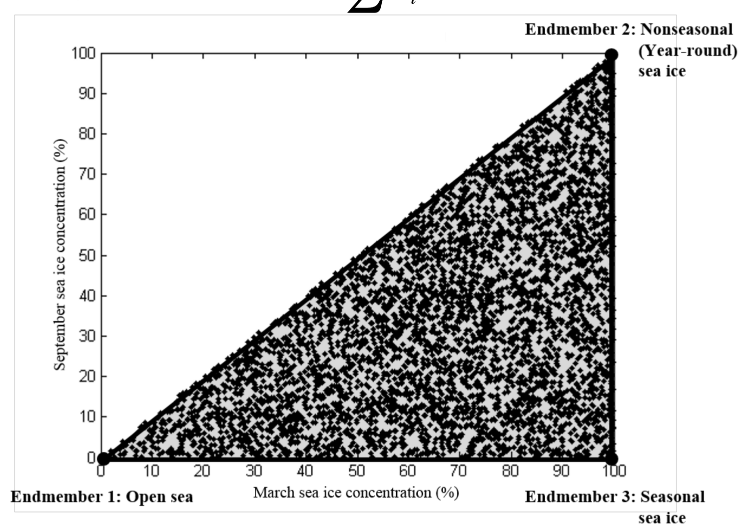

- Mixing effects on the multi-temporal SIC using three temporal EMs (Figure 1):
  1) Open sea: Sea ice free in both March and September.
  2) Non-seasonal sea ice: 100% sea ice cover in both March and September.
  3) Seasonal sea ice: 100% SIC in March and 0% in September.

Figure 1. Basic definition of the temporal EMs (Piwowar, Peddle, and Ledrew 1998).

2.4 Endmember extraction

- The most crucial task in both SMA and TMA is identifying an appropriate set of EMs to use in the modelling of at-sensor pixel spectra or temporal trajectories through a linear combination of the EMs.
- Because image-derived EMs have the advantage of being collected under the same conditions as the RS data, an ML-based EE algorithm was typically used.
- Assuming that pure ore extreme signatures are EMs, the notion of geometric convexity is natural and logical. Thus, this approach is the most popular and is used to develop a wide range of algorithms.
- N-FINDR (Winter 1999):
  1) Main idea: Use the simplex of maximum volume spanned by the EMs as a major criterion.
  2) Assumption: The volume defined by a simplex spanned by the purest pixels is grater than any other volume defined by any other combinations of pixels.
  3) Algorithm description:
     Step 1. Arbitrarily select initial seed points (EM candidates) $[\mathbf{e}_1, \mathbf{e}_2, \ldots, \mathbf{e}_q]$.
     Step 2. Compute the volume (V) of the resulting simplex spanned by the seed points as follows:

$$V(\mathbf{e}_1,\mathbf{e}_2,\cdots,\mathbf{e}_q)=\left|\det\left(\begin{bmatrix} 1 & 1 & \cdots & 1 \\ \mathbf{e}_1 & \mathbf{e}_2 & \cdots & \mathbf{e}_q \end{bmatrix}\right)\right| / (q-1)!$$

     Step 3. Evaluate the volume for each pixel to replace each EM position as a new simplex vertex until no larger simplex is found, as follows:

$$\arg \max_{(\mathbf{e}_1,\mathbf{e}_2,\cdots,\mathbf{e}_q)} V(\mathbf{e}_1,\mathbf{e}_2,\cdots,\mathbf{e}_q)$$

* N-FINDR requires dimensionality reduction because the matrix $\begin{bmatrix} 1 & 1 & \cdots & 1 \\ \mathbf{e}_1 & \mathbf{e}_2 & \cdots & \mathbf{e}_q \end{bmatrix}$ must be a square matrix for its determinant to exist. In this study, the maximum noise fraction (MNF) transform was used.

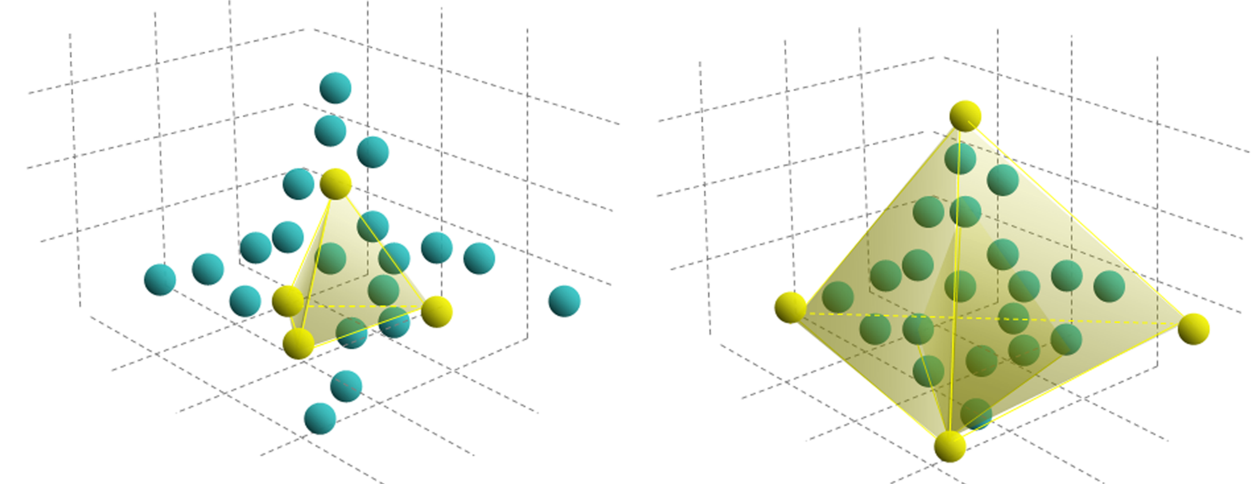

Figure 2. Graphical interpretation of the N-FINDR algorithm in a 3-dimensional space. (Left) N-FINDR initialized randomly (q=4) and (Right) final volume estim ation by N-FINDR (Remón *et al.* 2013).

3. Experimental results

- The N-FINDR algorithm identified the representative nine temporal EMs and the corresponding fractional abundances associated with the temporal EMs, as shown in Figure 3 and Figure 4, respectively.
- The fractional abundance maps of the extracted temporal EMs represent the spatial distribution of sea ice during a particular season and provide a quick summary of the temporal characteristics of hypertemporal SIC data for each year.

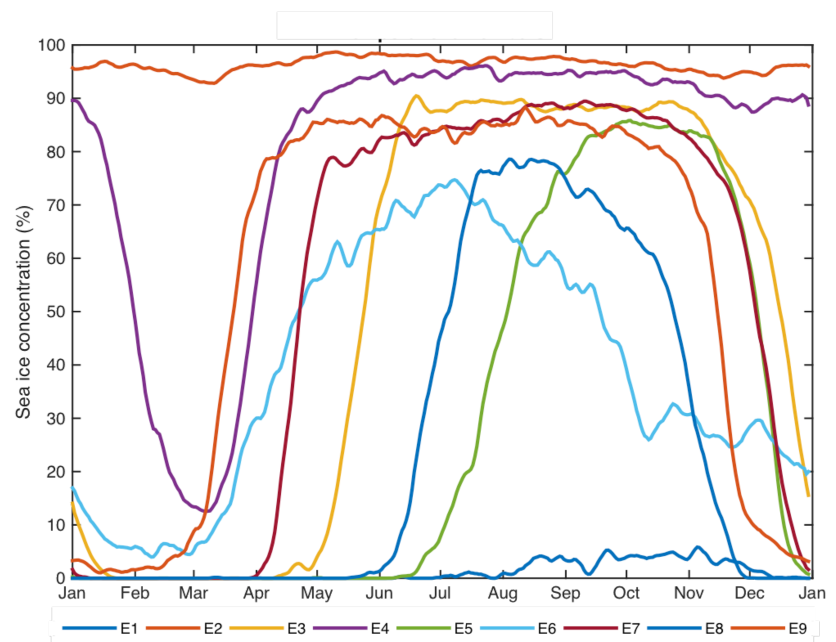

Figure 3. Extracted temporal EMs showing the variation in sea ice concentration throughout the year.

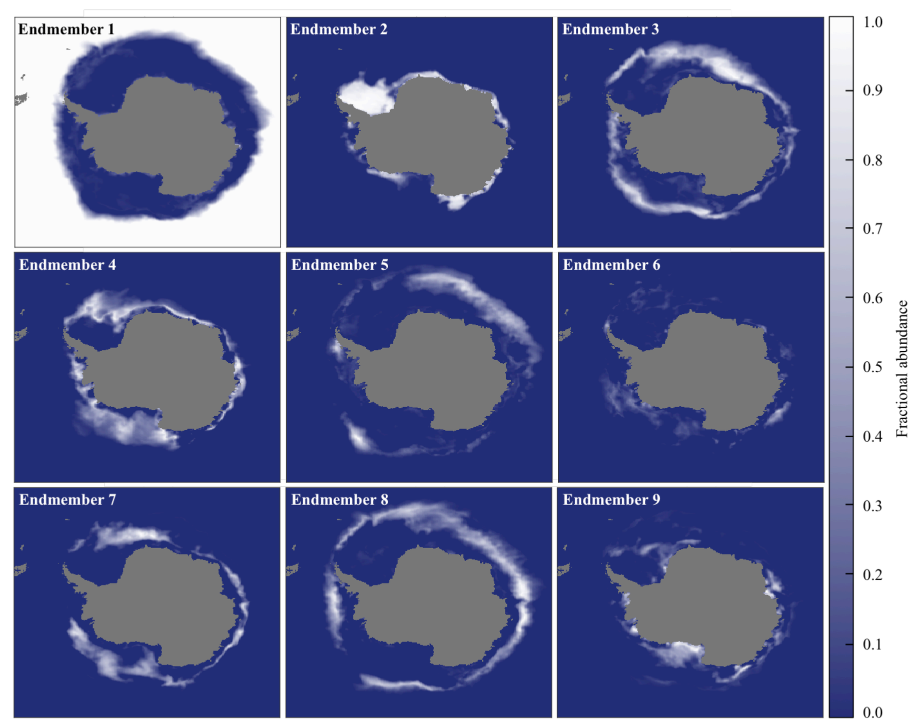

Figure 4. Fractional abundance maps of temporal EMs (E1-E9).

3.1 Reconstruction image comparison

- The HTI can be reconstructed via the inverse process of pixel unmixing.
- Although a combination of the temporal EMs and the corresponding fractions does not always ensure perfect reconstruction, it can be used, to a certain, to create reference images that do not contain anomalies from other unexpected environmental factors and that mitigates the impact of processing error noise.
- The reconstructed images did not capture the detailed variability in the local areas as shown in Figure 5; however, they generally exhibited better visual consistency with the original images.

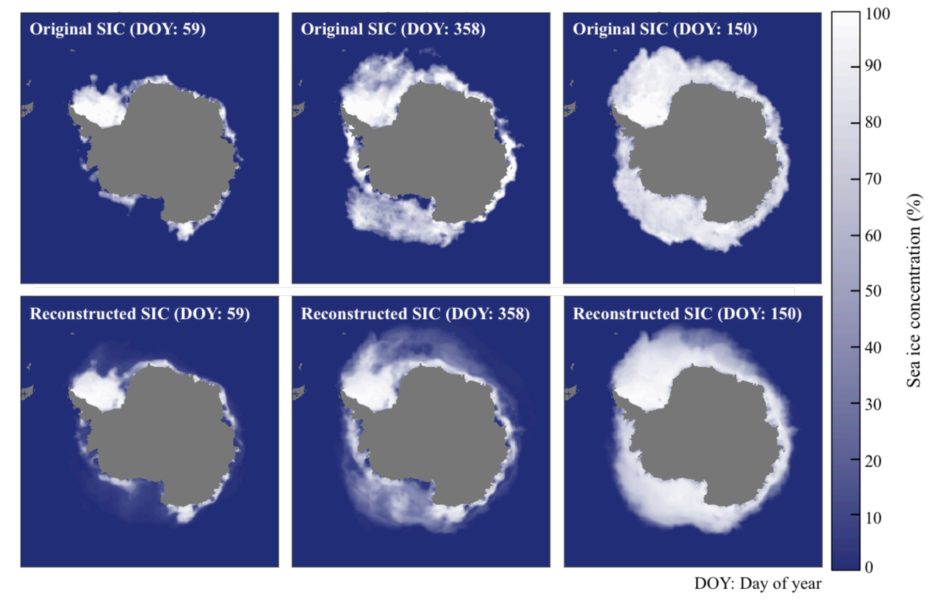

Figure 5. Comparison of the original SIC with the reconstructed data. (Left) Best fit (RMSE 3.6%), (Middle) worst fit (RMSE 9.2%) and (Right) mean fit (RMSE 6.9%)

3.2 Regional comparison

- While the Arctic SIC exhibits a long-term negative trend, the overall Antarctic sea ice has been expanding for decades. However, SICs exhibit great spatial variability in the Antarctic. The sea ice has significantly increase in the Ross Sea, while the Amundsen Sea sector exhibits a negative trend.

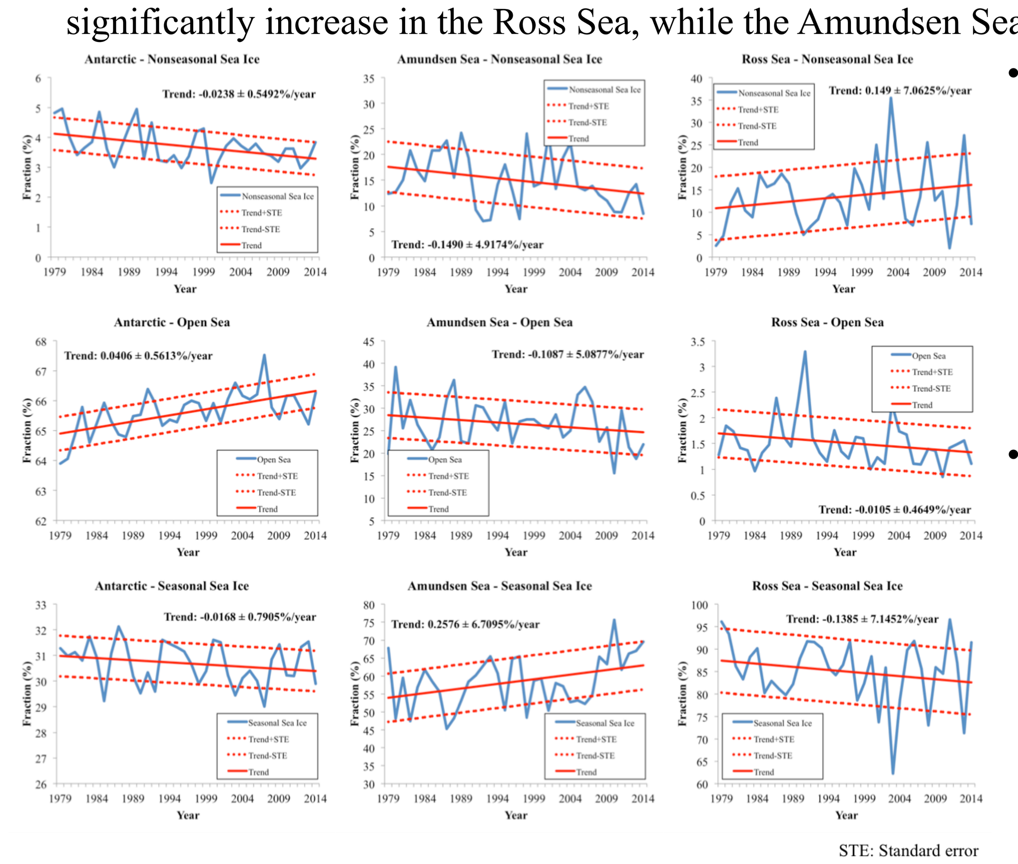

Figure 6. Regional comparison of non-seasonal sea ice, open water and seasonal sea ice in (Left) the entire Antarctic, (Right) the Ross Sea and (Middle) the Amundsen Sea.

- The slopes of three trend lines over the extent of the whole of the Antarctic sea ice were less steep than those for the Ross and the Amundsen Seas, which indicates that none of the three temporal signatures was significantly affected by the overall sea ice increase in the Antarctic (Figure 6(Left)).
- Sea ice in the Ross Sea has exhibited a more significant change in annual average than the southern hemisphere average has. Year-round SIC in the Ross Sea exhibits a positive trend; however, the area of open water has not changed significantly, and seasonal SIC exhibits a negative trend. These data indicate that sea ice growing in the Ross Sea sector is attributable to non-seasonal sea ice rather than open water or seasonal sea ice (Figure 6(Right)).
- Unlike the Ross Sea, the Amundsen Sea sector has exhibited statistically significant decreases in SIC. The TMA results show negative trends in both non-seasonal sea ice and open water in the Amundsen Sea. However, the trend for multi-year ice shows a significant negative trend compared with the southern hemisphere and Ross Sea, while the extent of seasonal sea ice exhibits a positive trend. Overall, these results indicate that a decrease in the non-seasonal sea ice fraction in the Amundsen directly affects the declining levels of sea ice, and considerable areas of multi-year ice and sea ice-free regions in the Amundsen have transitioned to areas of seasonal sea ice (Figure 6(Middle)).

4. Conclusions and future work

- Three conclusions were derived from this study:
  1) TMA efficiently provides a unique summary of long-term time series.
  2) The reconstructed images did not frequently contain or minimize the impact of anomalies.
  3) The changes in fractional abundances for each temporal EM in each region explained the overall impact of seasonal sea ice on the sea ice changes in each region.
- Several challenges remain to motivate future research:
  1) NSIDC's SIC data and retrieval algorithms should be evaluated for more scientific purposes.
  2) Spatial information, which is distinguishing characteristics of image data, should be exploited to yield more accurate EM signatures.
  3) An ensemble of the TMA results and other environmental factors might be used to better interpret sea ice dynamics in the Antarctic.

References

Heinz, D. C., and C.-I. Chang. 2001. "Fully Constrained Least Squares Linear Spectral Mixture Analysis Method for Material Quantification in Hyperspectral Imagery." IEEE Transactions on Geoscience and Remote Sensing 39 (3): 529–545.
Piwowar, J. M., D. R. Peddle, and E. F. Ledrew. 1998. "Temporal Mixture Analysis of Arctic Sea Ice Imagery: A New Approach for Monitoring Environmental Change." Remote Sensing of Environment 63 (3): 195–207.
Remón, A., S. Sánchez, S. Bernabé, E. S. Quintana-Ortí, and A. Plaza. 2013. "Performance Versus Energy Consumption of Hyper-spectral unmixing algorithms on multi-core platforms." EURASIP Journal on Advances in Signal Process 2013 (68).
Winter, M. E. 1999. "N-FINDR: An Algorithm for Fast Autonomous Spectral End-Member Determination in Hyperspectral Data." SPIEs International Symposium on Optical Science, Engineering, and Instrumentation, Denver, CO, July 18, 266–275.

** This study was supported by the Korea Polar Research Institute [grant number PE15040].